Energy loss of heavy ions specularly reflected from surfaces under glancing-angle incidence

Yuan-Hong Song* and You-Nian Wang
The State Key Laboratory of Materials Modification by Laser, Electron, and Ion Beams, Department of Physics, Dalian University of Technology, Dalian 116023, People's Republic of China

Z. L. Mišković
Department of Applied Mathematics, University of Waterloo, Waterloo, Ontario, Canada N2L 3G1
(Received 6 July 2000; published 17 April 2001)

A theoretical model is developed to study the energy loss of heavy ions specularly reflected on a solid surface at a glancing angle using the dielectric response theory and the specular reflection model. A local-field correction and a plasmon-pole approximation for dielectric function are employed in the low- and high-velocity regimes, respectively. Also, the Brandt-Kitagawa model is used to express the distribution of the electrons bound to the projectiles. We obtain analytical expressions for the position-dependent stopping power and the surface image potential. The energy losses, dependent on the charge state of the ions and the incident angles, are calculated and compared with the corresponding experimental results.

DOI: 10.1103/PhysRevA.63.052902 PACS number(s): 34.50.Dy, 34.50.Bw, 61.80.−x

I. INTRODUCTION

Extensive studies have focused recently on the interaction of heavy ions with solids, both experimentally and theoretically. Especially multiply charged ions, which are available due to rapid progress in the development of ion sources, are of interest in such areas as ion scattering spectroscopy, electron emission, x-ray emission and sputtering [1–4], where inelastic loss processes, charge exchange, ionization, and neutralization are studied.

When an energetic ion with a positive charge approaches a metal surface or a crystal surface under a grazing angle, it will be first attracted by a long-ranged induced electric field due to excitations of the electron gas in the surface and subsequently reflected by a short-ranged repulsive force of atoms located in the first surface layer. By studying the scattering trajectory and the energy loss of the ion, one can obtain an information about the structure of the solid surface. During the past few years, many authors have calculated and measured energy losses for light ions such as protons, specularly scattered on solid surfaces under grazing incidence [5–12]. For heavy-ion scattering, however, one should consider the effects of the charge state of the projectiles on the energy loss. In this case, the evolution of the projectile charge state due to the neutralization and ionization processes is very complex. Generally, the charge state depends on the projectile velocity, the incident angle, and the distance between the ion and the solid surface.

For a slow, highly charged ion moving near a solid surface, the charge transfer occurs mainly through resonant and Auger processes, while the energy loss of the ion is dominated by the excitation of electrons in the valence band of the solid. A theoretical analysis of the neutralization dynamics above the surface has been presented on the basis of the classical over-the-barrier (COB) model [13] in which resonant multielectron capture of conduction electrons, resonant loss into the unoccupied states of the conduction band, and the intra-atomic Auger deexcitation were considered and the transient formation of hollow atoms was described. For grazing incidence, the staircase model of sequential neutralization has been formulated as a simplified analytical treatment of the COB model [14,15], which was recently extended in a simulation of the neutralization processes above the conducting and insulating surfaces [16]. Winecki, and co-workers [17–19] have measured the energy loss and the final average charge states for C^{q+}, Ar^{q+}, and Fe^{q+} ions after grazing scattering from a smooth graphite surface and introduced a simple model of the neutralization of argon projectiles at low impact velocities. They found that the energy losses and the final charge states are almost independent of the initial charge state of the ion, which makes clear that the ion experiences a charge-state equilibration during the grazing scattering and attains a full neutralization before it reaches the distance of the closest approach. Based on an analytical approximation, a position-dependent stopping power has been obtained in a simple exponential form for slow ions during grazing scattering showing pronounced oscillations with Z_1 [20]. Based on the experimental data, which show a monotonic increase of the energy loss of N^{q+} ions with increasing charge state and the calculations of the stopping of N^{q+} ions for different charge states, an effective distance from the surface at which the ion is fully neutralized and relaxed has been estimated in Refs. [21,22].

For grazing scattering of high-velocity heavy ions on solid surfaces, the experimental data are less abundant than for slow ions, while, to the best of our knowledge, no theoretical studies of the ion charge states and the energy losses seem to be available. For 2-MeV C^{3+} and C^{4+} ions incident on SnTe crystal surfaces under glancing angles, Fritz *et al.* [23] have measured the energy losses and the charge-state distributions and deduced from the experimental data, effective ion charges and a freezing distance at which the ions begin to change their charge states.

In our previous work [5], grazing scattering of protons from a solid surface has been investigated based on the di-

*Email address: songyh@dlut.edu.cn

electric response theory and the specular reflection model (SRM) [24,25], and the numerical results for energy losses have been obtained that agree well with the corresponding experimental data. In the present paper, we develop a theoretical model to simulate the position-dependent stopping power, the scattering trajectory and the energy loss for heavy-ion grazing scattering on a solid surface. The organization of the paper is as follows. In Sec. II, general expressions for the surface image potential and the stopping power are formulated on the basis of the SRM in conjunction with the dielectric response theory taking into account the distribution of electrons bound to the projectile. In Sec. III, numerical results for energy losses of ions are obtained and compared with the available experimental data in both the low- and the high-velocity regimes. A short summary will be presented in Sec. IV. Atomic units (a.u.) will be adopted throughout this paper, where $m_e=\hbar=e=1$.

II. SURFACE IMAGE POTENTIAL AND STOPPING POWER

Assume an ion incident on a solid surface under a small glancing angle θ. A coordinate system is placed in the scattering plane with the x axis parallel to the surface and the z axis perpendicular to it. The scattering center ($x=0$, $z=0$) is placed at a target-atom nucleus in the first atomic plane such that the region $z<r_d$ is occupied by the electron gas of the bulk of the solid, where r_d is the average atomic radius of the target. The notations $\mathbf{r}=(\mathbf{R},z)$, $\mathbf{k}=(\mathbf{Q},k_z)$, and $\mathbf{v}=(\mathbf{v}_\parallel,v_z)$ will be used, where $\mathbf{R}$, $\mathbf{Q}$, and $\mathbf{v}_\parallel$ represent components parallel to the surface. In the vicinity of the surface, the ion is attracted by a force due to excitations of the electron gas and as a result its perpendicular velocity component v_z will increase. As the ion approaches the first atomic plane, the repulsive forces will become stronger than the attractive one and the ion will be specularly reflected by a collective planar potential. We only consider here the situation when the projectiles are reflected from the first atomic layer so that the angles of the incidence θ should be of the order of mrad. This in turn implies that we may assume that the ion moves parallel with the surface when the surface image potential and the stopping power are considered. This adiabatic dependence on the ion distance z_0 from the surface allows one to express the distribution of electrons bound at the ion as

$$\rho_{ext}(\mathbf{r},t)=[Z_1\delta(\mathbf{R}-\mathbf{v}_\parallel t)-\sigma_n(\mathbf{R}-\mathbf{v}_\parallel t)]\,\delta(z-z_0), \quad (1)$$

where Z_1 is the atomic number of the projectile and $(\mathbf{v}_\parallel t,z_0)$ is the position vector of the ion. Here, $\sigma_n(\mathbf{R})=\int\rho_n(\mathbf{r})dz$ is the two-dimensional charge distribution with $\rho_n(\mathbf{r})$ being the charge density of the bound electrons. Using a statistical model, an analytical expression for the charge density $\rho_n(\mathbf{r})$ was introduced by Brandt and Kitagawa (BK) [26], which we use here to express the Fourier transform of the external charge density as follows:

$$\tilde{\rho}_{ext}(\mathbf{k},\omega)=2\pi\tilde{\sigma}_n(Q)\,\delta(\omega-\mathbf{Q}\cdot\mathbf{v}_\parallel)e^{ik_zz_0}, \quad (2)$$

where, according to the BK model, $\tilde{\sigma}_n(Q)=Z_1[q(z_0)+(Q\Lambda)^2]/[1+(Q\Lambda)^2]$ with Λ being a screening length [26], $q(z_0)=1-N_n(z_0)/Z_1$ the ionization degree, and $N_n(z_0)$ the number of electrons bound at the ion located at z_0.

In order to describe the surface response, Ritchie and Marusak [24] and Wagner [25] introduced the SRM in which the induced potential can be determined by the external charge, its image and a fictitious surface charge fixed by the boundary conditions. Using the SRM and the dielectric response theory, the potential induced by the ion can be written in the form

$$\Phi_{ind}(\mathbf{r},t)=\frac{1}{2\pi}\int\frac{d\mathbf{Q}}{Q}\tilde{\sigma}_n(Q)F(Q,\omega,z',z_0')e^{-i\mathbf{Q}\cdot(\mathbf{R}-\mathbf{v}_\parallel t)}, \quad (3)$$

where $\omega=\mathbf{Q}\cdot\mathbf{v}_\parallel$ and $z'=z-r_d$, $z_0'=z_0-r_d$ are the positions along the z axis measured from the electron-gas edge of the solid surface, while $F(Q,\omega,z',z_0')$ is the interacting function. When the ion moves in vacuum ($z_0'>0$) and $z'>0$, the function $F(Q,\omega,z',z_0')$ can be expressed as

$$F(Q,\omega,z',z_0')=\frac{\epsilon_s(Q,\omega)-1}{\epsilon_s(Q,\omega)+1}e^{-Q(z'+z_0')}, \quad (4)$$

while for the ion traveling in the interior of the solid ($z_0'<0$) and $z'<0$, one obtains

$$F(Q,\omega,z',z_0')=\epsilon_s(Q,\omega,z'-z_0')+\epsilon_s(Q,\omega,z'+z_0')-\frac{2\epsilon_s(Q,\omega,z_0')\epsilon_s(Q,\omega,z')}{1+\epsilon_s(Q,\omega)}-e^{-Q|z'-z_0'|}, \quad (5)$$

with $\epsilon_s(Q,\omega,z')$ being the surface dielectric function, which can be expressed in terms of the bulk dielectric function $\epsilon(k,\omega)$ [27].

It will be shown that the surface image potential, i.e., the classical self-energy of the ion, is an important quantity in determining the ion trajectory. With the induced potential, Eq. (3), the surface image potential $U_s(z_0)=(1/2)\int d\mathbf{r}\rho_{ext}(\mathbf{r},t)\Phi_{ind}(\mathbf{r},t)$ can be expressed as

$$U_s(z_0)=\frac{1}{4\pi}\int\frac{d\mathbf{Q}}{Q}[\tilde{\sigma}_n(Q)]^2F(Q,\omega,z_0',z_0'). \quad (6)$$

With the x axis along the direction of the parallel component of the ion velocity $\mathbf{v}_\parallel\simeq\mathbf{v}$, and using the induced surface potential, Eq. (3), the position-dependent stopping power $S_e(z_0)=\int d\mathbf{r}\rho_{ext}(\mathbf{r},t)\mathbf{v}\cdot\nabla_{\mathbf{r}}\Phi_{ind}(\mathbf{r},t)/v$ is given by

$$S_e(z_0)=\frac{1}{2\pi v}\int\frac{d\mathbf{Q}}{Q}[\tilde{\sigma}_n(Q)]^2(-\mathbf{Q}\cdot\mathbf{v})\mathrm{Im}[F(Q,\omega,z_0',z_0')]. \quad (7)$$

Equations (6) and (7) present general expressions for the surface image potential and the stopping power, depending on both the projectile ionization degree $q(z_0)$ and the dielec-

tric function $\epsilon(k,\omega)$ of the matter. We note that no choice has been made so far for the dielectric function and the ionization degree. In the next section, two different forms of the dielectric function will be used to calculate the surface image potential and the stopping power for low- and high-velocity projectiles. The parametrized expressions for the ionization degree will be also presented in both the cases.

III. ENERGY LOSSES

Total energy loss of a heavy ion can be obtained by integrating the position-dependent stopping power, Eq. (7), along the scattering trajectory,

$$\triangle E = 2\int_{z_m}^{\infty} S_e(z_0)[1+(dz_0/dx)^{-2}]^{1/2}dz_0, \tag{8}$$

where z_m is the distance of closest approach to the scattering center. In the laboratory coordinate system, the trajectory equation for the projectile can be expressed as [5]

$$\frac{dz_0}{dx} = \mp\theta\sqrt{1-\frac{U_p(z_0)+U_s(z_0)}{E\theta^2}}, \tag{9}$$

where $E=mv^2/2$ is the initial kinetic energy of the incident ion, m is the mass of the ion, $U_p(z_0)$ is the surface continuum potential that can be obtained from the Molière's approximation [28], and $\mp$ correspond to the incoming and the outgoing trajectories. In Eq. (8), the closest distance z_m for the ion from the scattering center is given by the equation $E\theta^2 = U_p(z_m)+U_s(z_m)$. On integrating Eq. (9), one easily obtains a symmetrical trajectory of the ion. Generally, as we all know that, the incoming and the outgoing trajectories are not symmetrical strictly due to the distribution of the bound electrons of the projectiles. However, we also know, the projectiles will lose their energy mostly near and in the electron gas. So, our assumption of regarding the scattering trajectory as a symmetrical one is feasible while considering that the incident angles are of the order of mrad and the depth the ions enter into the target is no more than its average atomic radius r_d.

A. Low-velocity approximations

When the projectile velocity v is less than the Fermi velocity, $v_F=(3\pi^2 n_0)^{1/2}$, of the electron gas with density n_0, one can go beyond the random-phase approximation (RPA) [29,30] by using the local-field corrected (LFC) dielectric function [31,32], which provides a more accurate description of the excitations of the surface electron gas by including the exchange-correlation interaction among the electrons. Using the low-velocity approximation along with the LFC bulk dielectric function, the surface dielectric function $\epsilon_s(Q,\omega,z)$ can be expressed as

$$\epsilon_s(Q,z,\omega) = f_r(\kappa,z)+iuf_i(\kappa,z), \tag{10}$$

where $\kappa=Q/(2k_F)$ and $u=\omega/(\kappa v_F)$ are the dimensionless variables, $k_F=v_F$ is the Fermi wave number, while the detailed expressions for $f_r(\kappa,z)$ and $f_i(\kappa,z)$ are provided in [32]. On using Eq. (10) in Eq. (6), one can obtain the analytical expressions for the surface image potential in the vacuum ($z_0'>0$),

$$U_s(z_0) = k_F\int_0^1 d\kappa[\tilde{\sigma}_n(\kappa)]^2\frac{f_r(\kappa)-1}{f_r(\kappa)+1}e^{-4k_F\kappa z_0'} \tag{11}$$

and in the bulk of the solid ($z_0'<0$)

$$U_s(z_0) = k_F\int_0^1 d\kappa[\tilde{\sigma}_n(\kappa)]^2\Bigg[f_r(\kappa)+f_r(\kappa,2z_0') - \frac{2f_r^2(\kappa,z_0')}{1+f_r(\kappa)}-1\Bigg]. \tag{12}$$

Similarly, on using Eq. (10) in Eq. (7), the position-dependent stopping power can be expressed as

$$S_e(z_0) = 2k_F^2\frac{v}{v_F}\int_0^1 \kappa d\kappa[\tilde{\sigma}_n(\kappa)]^2 H(\kappa,z_0'), \tag{13}$$

in terms of the function

$$H(\kappa,z_0') = \frac{2f_i(\kappa)}{[1+f_r(\kappa)]^2}e^{-4k_F\kappa z_0'}, \quad z_0'>0, \tag{14}$$

or

$$H(\kappa,z_0') = f_i(\kappa)+f_i(\kappa,2z_0')+\frac{2f_r^2(\kappa,z_0')f_i(\kappa)}{[1+f_r(\kappa)]^2} - \frac{4f_r(\kappa,z_0')f_i(\kappa,z_0')}{1+f_r(\kappa)}, \quad z_0'<0, \tag{15}$$

where $f_r(\kappa)=f_r(\kappa,0)$, $f_i(\kappa)=f_i(\kappa,0)$, while a cutoff $\kappa=1$ has been introduced in the upper limit of the integral in Eq. (13).

As the projectile approaches the surface, it generally experiences electron capture and loss processes due to collisions with the surface atoms, but the evolution of the ionization degree in grazing scattering is not well understood at present. It has been observed in many experiments [17–19] that the low-velocity ions are largely neutralized by electron transfer from the metal surface before they reach the distance of the closest approach. In the present simulation, we adopt an exponentially decaying function to model the electron transition rate [33] when the ions are outside the electron gas. Thus, the position-dependent ionization degree can be expressed as a double exponent when $z_0>r_d$, viz.,

$$q(z_0) = q_0\exp\left\{-\exp\left(-\frac{z_0-z_s}{L}\right)\right\}, \tag{16}$$

where q_0 is the initial ionization degree and L is a characteristic length, while $z_s=L\ln(\Gamma_0 L/v_n)$, with v_n being the perpendicular velocity and Γ_0 a typical resonant ionization rate, which is taken to be of the order of 10^{15} s^{-1}. The determi-

nation of this parameter complies with Ref. [33], and we have testified that even two times larger or smaller value of it has few effects on our calculation results. And one can verify that the rate of change of the ionization degree $q(z_0)$ has a maximum at the location $z_0=z_s$.

When the projectile enters the electron gas in the bulk of the solid, $z_0<r_d$, we adopt an empirical model [34] based on a velocity-dependent electron-stripping criterion in which the ionization degree shows a remarkably good agreement with experimental values for heavy ions in solids, viz.,

$$q_b=1-\exp(0.803y_r^{0.3}-1.3167y_r^{0.6}-0.381\,57y_r - 0.008\,983y_r^2), \tag{17}$$

where $y_r=v_r/Z_1^{2/3}$, with v_r being the ion velocity relative to the target-electron velocity, defined as follows

$$v_r=v\left(1+\frac{v_F^2}{5v^2}\right), \quad v\geqslant v_F,$$
$$v_r=\frac{3v_F}{4}\left[1+\left(\frac{2v^2}{3v_F^2}\right)-\frac{1}{15}\left(\frac{v}{v_F}\right)^4\right], \quad v<v_F. \tag{18}$$

Using the matching condition $q(r_d)=q_b$, it is easy to find the value of the position z_s and the corresponding value of the characteristic length L.

In Fig. 1, we plot the energy losses for slow N^{q+} ions with the velocities $v=0.45v_0$ and $0.63v_0$ (v_0 being the Bohr velocity) incident on an Al surface under a grazing angle of $\theta=12.2$ mrad versus the initial ion-charge states. Also shown are the corresponding experimental points from Ref. [21] and the calculation results by using RPA dielectric function that does not include the local-field corrections. Theoretical results for the energy loss show a slight increase with the increasing charge state and fit the experimental results reasonably well. In fact, it is found that for heavy ions at low velocities, the linear reponse theory based on RPA is not expected to be valid for such a strong perturbation ($Z_1^{2/3}v_0/v\gg1$). On the contrary, the density functional formalism has done a sound job in describing the response of the electron gas to this kind of perturbation by calculating the self-consistent potential that includes the result of the nonlinear screening of the ion and the exchange-correlation effect of the electron gas [35–37]. However, from Fig. 1, we have reasons to believe that after some corrections, the linear response theory is still applicable to be adopted at low velocities regime. These corrections in the present work include: the effects of the exchange-correlation interaction of electrons can be included approximately by a static LFC to the dielectric function that had already adopted in the researches of the wake potential and energy loss of an ion moving near a solid surface and in a solid [5,31,32,38]. It has been proved in Fig. 1 and our previous work [39] that the results of the stopping power calculated by LFC show increases over those based on RPA dielectric theory; on the other hand, the mean effect of all capture and loss processes is considered by the BK effective charge theory, cooperating with two different empirical expressions of the ionization degree based on the classical barrier model and experimental data, respectively.

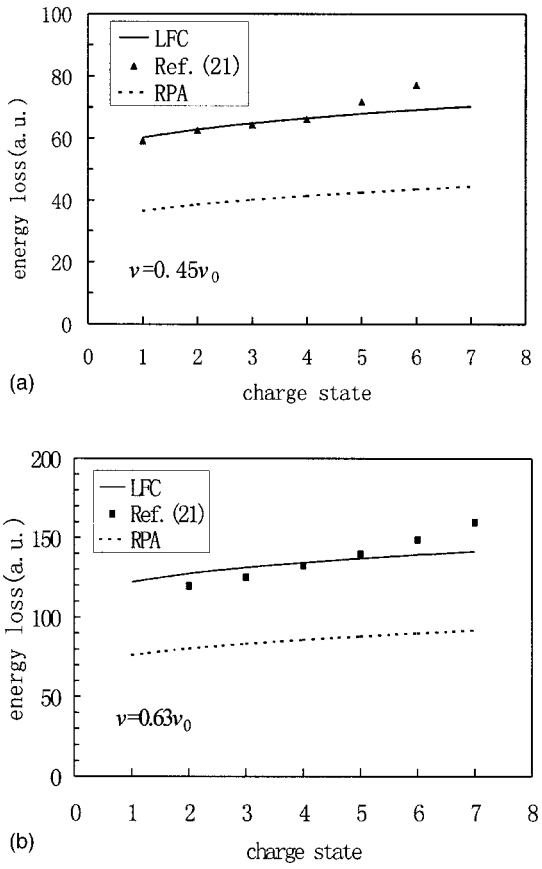

FIG. 1. Energy loss as a function of the incident charge for N^{q+} ions specularly reflected from an Al surface under an incident angle $\theta=12.2$ mrad (about 0.7°). The solid lines represent the calculation results of our model for the initial ion velocities of (a) $0.45v_0$ and (b) $0.63v_0$ (v_0 being the Bohr velocity). The triangles and the squares are the experimental values taken from Ref. [21], and the dashed lines are the results by using RPA dielectric function.

We have also calculated the energy loss as a function of increasing incident angles for different initial charge states of the ions, as shown in Figs. 2 and 3. As in our previous

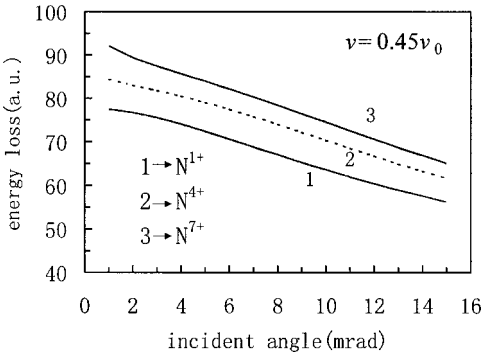

FIG. 2. Calculation results for energy loss of N^+, N^{4+}, and N^{7+} ions as a function of the incident angles for grazing scattering from an Al surface at an initial velocity of $v=0.45v_0$.

calculations for hydrogen ions at low velocities [5], one can easily see from these two figures that the energy losses decrease monotonously as the incident angles increase. In addition, the distances of the closest approach are presented in Fig. 4 in terms of the incident angles showing that the larger the incident angle, the deeper the ion penetrates into the electron gas located in the region $z_0 < r_d$ with the atomic radius $r_d = 2.99$. Intuitively, the energy loss should be most intense in the vicinity of the topmost layer giving rise to larger energy losses for shorter distances of closest approach and consequently, larger incident angles (see Fig. 4), which contradicts the trends in Figs. 2 and 3. In fact, a decrease in the distance of the closest approach does not imply an increase of the length of the projectile trajectory through the electron gas in the surface region. On the contrary, the attractive surface image potential increases the effective angle of incidence, thus making the effective length of the projectile trajectory through the electron gas shorter when the incident angles are larger. Thus, the trends shown in Figs. 2 and 3 for the energy loss as a function of the incident angle can be easily understood through the use of Eqs. (8) and (9). However, this conclusion does not tally well with Ref. [22] in which the energy losses show little dependence on the incident angles.

On the other hand, the ionization degree of the ion in the electron gas is obtained from Eq. (17) and, therefore, does not depend on the initial charge state. Thus, in Fig. 4, the closest distance, which is determined by the surface image potential and the surface continuum potential, depends only on the incident angles and the impact energy but not on the initial charge state.

B. High-velocity approximations

Several approximations to the bulk dielectric function have been used in literature to express the surface response to fast incident ions such as the hydrodynamic approximation and the plasmon-pole approximation (PLA) [27]. We have used recently the local frequency-dependent dielectric function with a damping factor to represent the response of the medium at high projectile velocities [5], where only the contributions of the collective excitations to the energy loss were considered. However, the contribution of single-electron excitations of the solid atoms should also be included especially for the projectiles at small distances from the surface. In this work, the PLA is adopted in which both of these two types of excitations are included, with

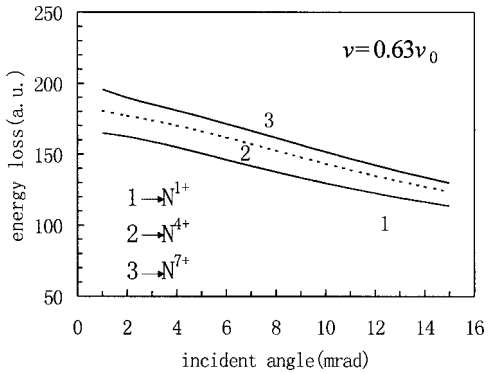

FIG. 3. Same as Fig. 2, except for the initial velocity $v = 0.63v_0$.

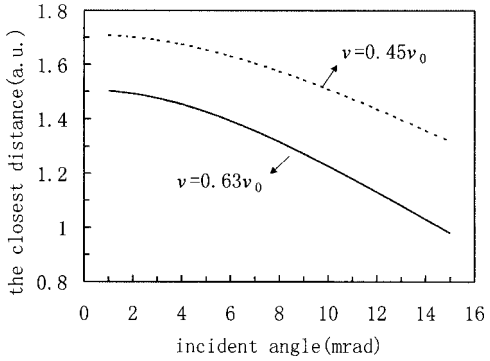

FIG. 4. Distance of closest approach to the surface topmost layer for N^{q+} ions specularly reflected at Al surface as a function of the incident angles. The solid line corresponds to the ion velocity $0.63v_0$ and the dashed line to the velocity $0.45v_0$.

$$\epsilon(k,\omega) = 1 + \frac{\omega_p^2}{k^4/4 + \beta^2 k^2 - \omega(\omega + i\gamma)}, \tag{19}$$

where $\beta = \sqrt{3/5} v_F$ is the speed of propagation of density disturbances in an electron gas characterized by a Fermi velocity v_F, ω_p is the plasma frequency of the medium, and γ is an infinitesimal positive quantity representing the damping of the plasma. In order to obtain analytical results, we assume that the dielectric function depends on k only through its component Q parallel to the surface. Such an approximation was proved to be a reliable one in Refs. [40,41] assuming that the plasmon dispersion along the z axis may be neglected, which is justified in our small incident-angle model. Thus, the surface dielectric function can be expressed as

$$\epsilon_s(Q,\omega,z_0') = \frac{e^{-Q|z_0'|}}{\epsilon(Q,\omega)}. \tag{20}$$

Similar to the work for point charges obtained by Echenique *et al.* [42], the surface image potential and the stopping power can be figured out as follows.

On using this expression for the surface dielectric function in Eq. (6), we obtain the analytical description of the surface image potential in the high-velocity approximation, viz.,

$$U_s(z_0) = -\frac{\omega_s^2}{2}\int_0^{\omega_s/v} dQ[\tilde{\sigma}_n(Q)]^2 \frac{1}{A_s\sqrt{A_s^2 - Q^2v^2}} e^{-2Q|z_0'|} - \Theta(-z_0')\frac{\omega_p^2}{2}\int_0^{\omega_p/v} dQ[\tilde{\sigma}_n(Q)]^2 \frac{1}{A_p\sqrt{A_p^2 - Q^2v^2}} \times (1 - e^{-2Q|z_0'|}), \tag{21}$$

where $\omega_s = \omega_p/\sqrt{2}$ is the surface plasma frequency, $A_s^2 = Q^4/4 + \beta^2Q^2 + \omega_s^2$, and $A_p^2 = Q^4/4 + \beta^2Q^2 + \omega_p^2$. The ana-

lytical expression of the stopping power can be obtained by using Eq. (20) in Eq. (7), in which case

$$Se(z_0)=\frac{\omega_s^2}{v}\int_{\omega_s/v}^{2v} dQ[\tilde{\sigma}_n(Q)]^2\frac{1}{\sqrt{Q^2v^2-A_s^2}}e^{-2Q|z_0'|}+\Theta(-z_0')\frac{\omega_p^2}{v}\int_{\omega_p/v}^{2v} dQ[\tilde{\sigma}_n(Q)]^2\frac{1}{\sqrt{Q^2v^2-A_p^2}}\times(1-e^{-2Q|z_0'|}). \quad (22)$$

In fact, when the velocity of the incident particle is much larger than those of the electrons in the solid, both the outer-shell electrons (homogeneous electron gas) and the inner-shell electrons will contribute to the energy loss. Contribution of the inner-shell electrons to the stopping power is calculated by using an approximate expression for the total electron density $n_e(z)$ [43] derived from the continuum surface planar potential in the form

$$n_e(z)=[Z_2N_p/(2a_{TF})]\sum_{i=1}^{3}\alpha_i\beta_i\exp(-\beta_i z/a_{TF}), \quad (23)$$

where Z_2 is the atomic number of the target atoms, N_p is the atomic density of the surface atomic plane, $a_{TF}=0.8853/Z_2^{1/3}$, $\{\alpha_i\}=\{0.1,0.55,0.35\}$, and $\{\beta_i\}=\{6.0,1.2,0.3\}$. This expression is used in the bulk contribution to the stopping power described by the second term in Eq. (22).

On the other hand, at high velocities, the ions may enter into the electron gas deeper in a shorter interaction time and be exposed to electron loss as well as electron capture when compared with the slow ions. The charge exchange in the vicinity of the topmost atomic layer will be so intense that the charge state will become equilibrated within a short path length [44], in agreement with the definition of a freezing distance at which the charge exchange processes begin to take place [23], which was shown to be almost independent of the incident angle and less than the atomic radius r_d. This means the exchange process of the ion-charge state might occur within the electron gas. Consequently, we adopt a picture where the charge state remains unchanged when the ion is outside the electron gas ($z_0>r_d$), while the ionization degree is given by Eq. (17) when the ion is close to the topmost layer ($z_0<d$). In order to describe the charge evolution, we use, somewhat arbitrarily, a linear interpolation between the initial charge state q_0 and the equilibrium bulk ionization degree q_b when the ion is in the range $d<z_0<r_d$ of distances from the surface, viz.,

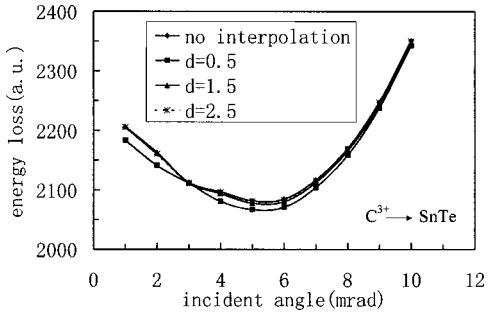

FIG. 5. Energy loss for C^{3+} ions scattered on the surface of SnTe as a function of the incident angles. The initial ion velocity is $2.583v_0$. One line corresponds to the case without the linear interpolation between q_0 and q_b and the other three lines correspond to different values of the parameter d at which the ion-charge state begins to follow Eq. (17).

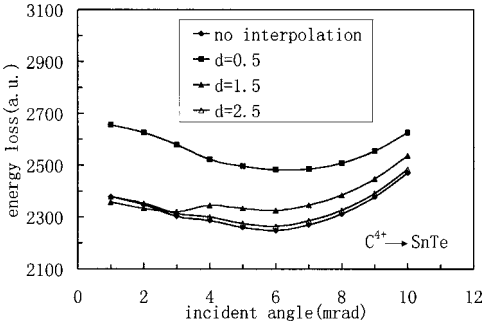

FIG. 6. Same as Fig. 5 except for the initial charge state: C^{4+} ions.

$$q(z_0)=q_0-\frac{r_d-z_0}{r_d-d}(q_0-q_b) \quad (24)$$

with d being a free parameter. Although such a description of the charge state evolution is rather qualitative, it will prove practical in subsequent calculations of energy losses in high-velocity ion-surface grazing scattering.

In order to compare our model with available experimental data [23], we simulate the energy loss of C^{q+} ions incident on the surface SnTe(100). The jellium edge in the SnTe is at $r_d=2.99$ a.u. from the topmost atomic layer [44] while the target charge Z_2 corresponding to the SnTe surface is approximated by $Z_2=(Z_{Sn}+Z_{Te})/2=51$, which is justified because the atomic numbers of Sn and Te are close enough. Figures 5 and 6 show the energy losses of C^{3+} and C^{4+} ions, respectively, in terms of the incident angles with the initial

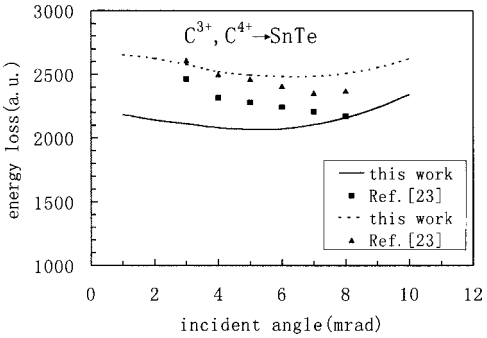

FIG. 7. Energy loss as a function of the incident angles for C^{3+} and C^{4+} ions specularly reflected from the surface of SnTe. The solid line shows the results for C^{3+} ions while the dashed line shows the results for C^{4+} ions, with the initial velocity of the ions being $2.583v_0$. The squares and the triangles are the experimental values taken from Ref. [23], corresponding to C^{3+} and C^{4+} ions, respectively.

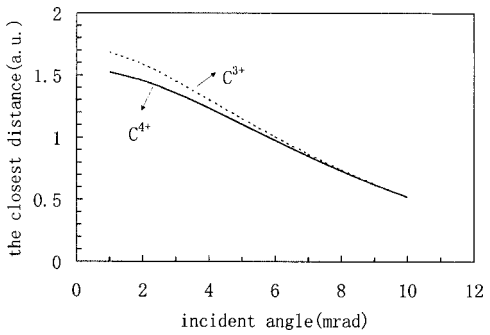

FIG. 8. Distance of closest approach to the surface topmost layer for C^{3+} and C^{4+} ions specularly reflected at SnTe surface as a function of the incident angles. The solid line corresponds to the case of C^{4+} and the dashed line to the case of C^{3+}.

velocity $v \simeq v_{\parallel} = 2.583 v_0$ for several values of the parameter d and even no linear interpolation. It should be noted that the variation in d exhibits strong effects in Fig. 6 for incident C^{4+} ions (with the initial ionization degree $q_0 = 2/3$) while almost no effects of a variable d are observed in Fig. 5 for C^{3+} ions (where $q_0 = 0.5$). On the other hand, at velocity $v = 2.583 v_0$, we obtain from Eq. (17) the ionization degree in the solid $q_b = 0.5096$, which agrees with the effective charge number $Q_f = 3.22$, obtained in Ref. [23] from a semianalytical model. Comparing these values to the initial ionization degrees in Figs. 5 and 6, one can conclude that the change of the ionization degree plays an important role in the case of scattering under the jellium edge. Finally, we choose $d = 0.5$ and calculate the energy losses in terms of the incident angles, which are displayed in Fig. 7 and compared with the corresponding experimental values from Ref. [23]. The calculated and measured data show an overall agreement while the discrepancies may be attributed to the crudeness of our modeling of ion-charge state evolution. We note that the inner-shell electron contributions to the stopping power have been taken into account in calculations shown in Fig. 7 giving rise to an increase of energy losses for larger incident angles, which was not observed in Fig. 1 for low ion velocities. This increase in energy loss with increasing incident angles for high-velocity ions was observed experimentally [12] and confirmed theoretically [5] for H^+, but is clearly absent in the experimental data for heavy ions, shown in Fig. 7. Finally, the distance of closest approach z_m is shown in Fig. 8 as a function of the incident angles. Since the C^{3+} and C^{4+} ions with the same incident velocity experience different degrees of charge exchange in the jellium, their trajectories are different at smaller incident angles but the fact that the ions attain the same equilibrium charge state in the vicinity of the topmost layer implies that they may penetrate to about the same depth when the incident angle is greater than about 7 mrad as shown in Fig. 8.

IV. SUMMARY

Based on the dielectric response theory and the specular reflection model, general expressions for the surface image potential, the position-dependent stopping powers, the projectile trajectories, and the energy losses have been presented for heavy-ions under grazing incidence on a solid surface. The LFC and PLA dielectric functions were adopted in the low- and the high-velocity regimes, respectively. The distributions of the electrons bound at the incident ions were taken into account by using the BK model. Our simulation requires a complete description of the position-dependent ionization degree throughout the scattering process, which is not known at present. Considering that the charge-exchange probabilities near the surface may be different for slow and fast projectiles, a double exponent model and a linear interpolation, both combined with a velocity-dependent electron-stripping model, were employed in simulations. Although such approximate treatments of the ion-charge evolution seem rather crude, they have proved to be practical in our calculations, corresponding to available experimental data.

In the low-velocity regime, calculations of the energy loss exhibit a monotonic increase with the increasing charge state, consistent with the data from Ref. [21], and show a slight decrease with the increasing incident angles. The calculated results demonstrate that both the charge state of the ions and the incident angles affect the ion scattering trajectory as well as the energy loss. On the other hand, high-velocity ions may approach the topmost layer much closer than slow ions as the incident angles increase so that the contribution of the inner-shell electrons to the stopping power should be included giving rise to a small increase of the energy loss when the incident angles are greater than 7 mrad as shown in Fig. 7. Such an effect was observed [12] and confirmed theoretically [5,6] for hydrogen ions, but was not found in the experimental data for heavier atoms [23]. Clearly, such a situation warrants a more complete research effort, both experimentally and theoretically.

ACKNOWLEDGMENTS

This work was jointly supported by the Research Fund for the Doctoral Program of Higher Education, the Fund for the Excellent Young Faculty, the Key Fund of the Science and Technology of the State Education Ministry, and the National Natural Science Foundation of China (Y.N.W.).

[1] R.J. MacDonald, D.J. O'Connor, J. Wilson, and Y.G. Shen, Nucl. Instrum. Methods Phys. Res. B **33**, 446 (1988).
[2] M.H. Shapiro and T.A. Tombrello, Nucl. Instrum. Methods Phys. Res. B **90**, 473 (1994).
[3] S.J. Timoner, M.H. Shapiro, and T.A. Tombrello, Nucl. Instrum. Methods Phys. Res. B **114**, 20 (1996).
[4] A. Arnau *et al.*, Surf. Sci. Rep. **27**, 113 (1997).
[5] Y.H. Song and Y.N. Wang, Nucl. Instrum. Methods Phys. Res. B **153**, 186 (1999).
[6] J.I. Juaristi, F.J. García de Abajo, and P.M. Echenique, Phys. Rev. B **53**, 13 839 (1996).
[7] K. Kimura, M. Hasegawa, and M. Mannami, Phys. Rev. B **36**,

7 (1987).
[8] H. Winter, J. Remillieux, and J.C. Poizat, Nucl. Instrum. Methods Phys. Res. B **48**, 382 (1990).
[9] F. Stölze and R. Pfandzelter, Surf. Sci. **251/252**, 383 (1991).
[10] R. Pfandzelter and F. Stölze, Nucl. Instrum. Methods Phys. Res. B **72**, 163 (1992).
[11] K. Narumi, Y. Fujii, K. Kishine, H. Kurakake, K. Kimura, and M. Mannami, Surf. Sci. **293**, 152 (1993).
[12] H. Winter, M. Wilke, and M. Bergomaz, Nucl. Instrum. Methods Phys. Res. B **125**, 124 (1997).
[13] J. Burgdörfer, P. Lerner, and F.W. Meyer, Phys. Rev. A **44**, 5674 (1991).
[14] J. Burgdörfer and F. Meyer, Phys. Rev. A **47**, R20 (1993).
[15] C. Lemell, H.P. Winter, F. Aumayr, J. Burgdörfer, and F. Meyer, Phys. Rev. A **53**, 880 (1996).
[16] J.J. Ducrée, F. Casali, and U. Thumm, Phys. Rev. A **57**, 338 (1998).
[17] S. Winecki, C.L. Cocke, D. Fry, and M.P. Stöckli, Phys. Rev. A **53**, 4228 (1996).
[18] S. Winecki, M.P. Stöckli, and C.L. Cocke, Phys. Rev. A **55**, 4310 (1997).
[19] S. Winecki, M.P. Stöckli, and C.L. Cocke, Phys. Rev. A **56**, 538 (1997).
[20] C. Auth, A. Mertens, and H. Winter, Nucl. Instrum. Methods Phys. Res. B **135**, 302 (1998).
[21] J.I. Juaristi, A. Arnau, P.M. Echenique, C. Auth, and H. Winter, Phys. Rev. Lett. **82**, 1048 (1999).
[22] J.I. Juaristi, A. Arnau, P.M. Echenique, C. Auth, and H. Winter, Nucl. Instrum. Methods Phys. Res. B **157**, 87 (1999).
[23] M. Fritz, K. Kimura, H. Kuroda, and M. Mannami, Phys. Rev. A **54**, 3139 (1996).
[24] R.H. Ritchie and A.L. Marusak, Surf. Sci. **4**, 234 (1966).
[25] D. Wagner, Z. Naturforsch, Z. Naturforsch. Teil A **21**, 634 (1966).
[26] W. Brandt and M. Kitagawa, Phys. Rev. B **25**, 5631 (1982).
[27] F.J. García de Abajo and P.M. Echenique, Phys. Rev. B **46**, 2663 (1992).
[28] Y. H. Ohtsuki, *Charged Beam Interaction with Solids* (Taylor & Francis, London, New York, 1983).
[29] J. Lindhard, Mat. Fys. Medd. K. Dan. Vidensk. Selsk. **28**, 8 (1954).
[30] F.J. García de Abajo and P.M. Echenique, Phys. Rev. B **48**, 13 399 (1993).
[31] Y.N. Wang and W.-K. Liu, Chem. Phys. Lett. **254**, 122 (1996).
[32] Y.N. Wang and W.-K. Liu, Phys. Rev. A **54**, 636 (1996).
[33] C.J. Setterlind and A. Bárány, Nucl. Instrum. Methods Phys. Res. B **98**, 407 (1995).
[34] J.F. Ziegler, J.P. Biersack, and U. Littmark, *The Stopping and Ranges of Ions in Matter* (Pergamon, Oxford, 1985), Vol. 1.
[35] P.M. Echenique, R.M. Nieminen, J.C. Ashley, and R.H. Ritchie, Phys. Rev. A **33**, 897 (1986).
[36] P.M. Echenique, Nucl. Instrum. Methods Phys. Res. B **27**, 256 (1987).
[37] J.I. Juaristi and A. Arnau, Nucl. Instrum. Methods Phys. Res. B **115**, 173 (1996).
[38] Y.H. Song and Y.N. Wang, Nucl. Instrum. Methods Phys. Res. B **135**, 124 (1998).
[39] Y.N. Wang and T.C. Ma, Nucl. Instrum. Methods Phys. Res. B **51**, 216 (1990).
[40] C.O. Reinhold and J. Burgdörfer, Phys. Rev. A **55**, 450 (1997).
[41] C. Denton, J.L. Gervasoni, R.O. Barrachina, and N.R. Arista, Phys. Rev. A **57**, 4498 (1998).
[42] P.M. Echenique, R.H. Ritchie, N. Barberán, and J. Inkson, Phys. Rev. B **23**, 6486 (1981).
[43] Y. Fujii, S. Fujiwara, K. Narumi, K. Kimura, and M. Mannami, Surf. Sci. **277**, 164 (1992).
[44] C.C. Montanari, M.S. Gravielle, V.D. Rodríguez, and J.E. Miraglia, Phys. Rev. A **61**, 022901 (2000).